The Mechanism of Low Ductility Failures of a Medium-Carbon Vanadium-Alloyed Steel

YU-TING TSAI, CHUNG-TAI LU, CHIU-WEN FANG and HERNG-SHUOH JANG

Iron and Steel Research and Development Department
China Steel Corporation

Vanadium forms fine VC precipitates in ferrite and pearlite under suitable cooling conditions, enhancing the strength of medium carbon steel. However, it was discovered that vanadium-alloyed medium carbon steels sometimes exhibited low elongations of 2-4%, and the tensile-fractured surface had a typical quasi-cleavage appearance. In this research, the cause of the brittle fracture is studied. It is shown that under tensile strain, the deformation of pearlitic structures follows the Miller-Smith mechanism, in which voids appear along shear bands, providing an easy route for crack propagation. Coarse prior austenite grains increase the extent of local stress concentrations, which is further weakened when the pearlite matrix is strengthened by VC precipitates. Therefore, both crack nucleation and propagation are promoted in coarse-grained vanadium-alloyed medium-carbon steel, resulting in low elongation.

Keywords: Vanadium, Steel, Tensile Test, Precipitation, Quasi-Cleavage Fracture

1. INTRODUCTION

The mechanical properties of steel are closely related to steel composition and heat treatment. For forging steel, typical tensile strength (TS) is shown in Figure 1. When the carbon concentration of the steel is between 0.2 to 0.4%, TS is about 500-700MPa. To enhance strength, the workpiece can be reheated, followed by quenching and tempering (QT), forming tempered martensite with a typical tensile strength of 800-1000MPa[2]. However, the reheating process is energy- intensive and increases CO_2 emissions. Furthermore, the quenching process causes distortion of the workpiece, and a costly machining process must be applied to achieve the required dimension.

Microalloying elements, such as Ti, Nb, and V, actively combine with carbon, forming MCN precipitates[(3)], where M stands for Ti, Nb, and V while C and N are carbon and nitrogen. MCN significantly modifies the microstructure and mechanical properties of steels. Compared to Ti, and Nb, vanadium is favorably used in medium carbon steel because of higher Vanadium carbide (VC) solubility during reheating. Upon cooling, vanadium forms small VC precipitates in ferrite/pearlite[(4,5)], increasing the strength of V-containing steels. With the small amount of V addition, as-forged workpiece can achieve 600-900 MPa with 10% elongation (EL) for a 0.4C% steel[(1)], comparable to QT steel, therefore QT treatment can be omitted, reducing overall production cost.

Recently, it was found that some hot forged parts have a low EL of 2-4%, which could potentially result in premature failure during service. To resolve the issue, the cause of low EL in vanadium-alloyed steel is investigated.

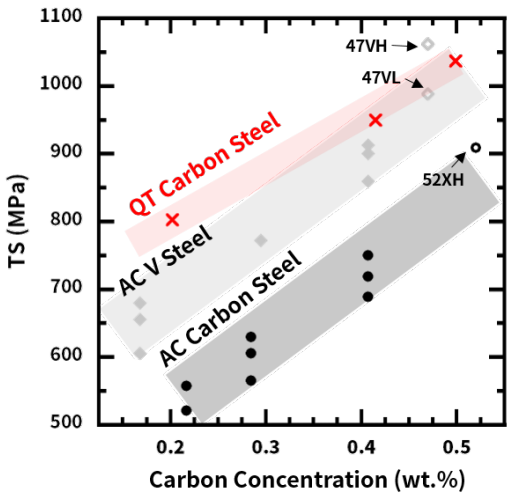

Fig.1. The relationship between tensile stress and carbon concentration of as-forged and air-cooled (AC) carbon steels or V-alloyed steels (V steel)[(1)]. Quenched and tempered (QT) carbon steels are also shown[(2)].

2. EXPERIMENTS

The samples were provided by a customer of China Steel Corporation. The chemical composition is shown in Table 1. The carbon concentrations of the samples are between 0.47, and 0.52%, and samples are hereafter referred to as 47V and 52X, where V/X indicates if there is a V addition. The bars were reheated between 1000-1200ºC, and the suffix H/L refers to higher/lower in this temperature range. After reheating, the bars were subsequently hot forged into workpieces, followed by air cooling to room temperature. Tensile samples were taken from a 1/4D position, the results are shown in Table 1. Standard metallographic procedures were applied to investigate the microstructure. TEM samples were carbon replicas, taken from gently etched metallographic specimens. Thermodynamic calculations were conducted using Thermal-Calc with the TCFE12 database.

3. RESULTS AND DISCUSSION

The mechanical properties of as-forged samples are shown in Table 1, and the elongation of 47VH is only 3.5% while 47VL is 11.9%. The optical micrographs are shown in Figure 2, the microstructures consisted of ferrite and pearlite, typical of forged medium carbon steel. As ferrite delineated prior austenite grain (PAG) boundaries, PAG size (PAGS) could be estimated using Figure 2, and the PAGS for 47VH and 47VL were >100μm and 75μm, respectively, which could be explained with the reheat temperature. Figure 3(a) shows the fracture surface of 47VH after tensile tests. The surface showed a rosette pattern, typical of quasi-cleavage, indicating brittle fracture. The unit of quasi-cleavage approximates PAGS, as shown in Figure 3(b), and the crack only deviated by PAG boundaries. With the results above, it seemed intuitive to conclude that deteriorated elongation was related to the difference in PAGS. Previous research also showed that, for a 0.8% eutectoid steel, when the PAGS was coarsened from 43μm to 227μm[6], EL was reduced from 11% to 6%. Additional experiments were conducted on 52XH, with a similar microstructure and exceptionally large PAG as

Table 1 Sample composition and mechanical properties

Sample	C	Si	Mn+Cr	V	Ti	Reheat Temperature	YS	TS	EL
47VH	0.47	0.27	1.74	added	<100ppm	High (H)	713	988	3.5
47VL						Low (L)	755	1062	11.9
52XH	0.52	0.26	1.76	-		High (H)	516	909	12.1

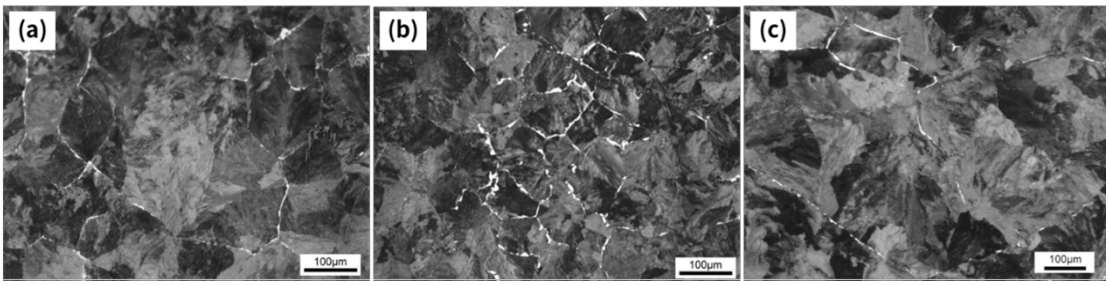

Fig.2. The microstructure of as forged (a) 47VH, (b) 47VL, and (c) 52XH.

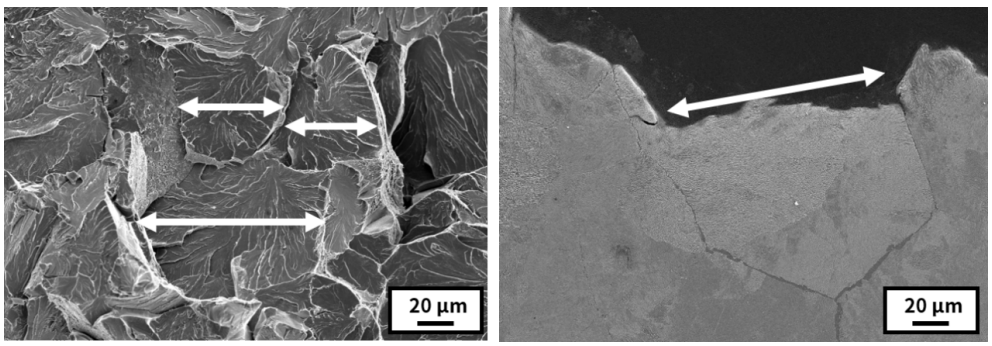

Fig.3. The fracture surface and profile of 47VH after tensile tests.

47VH. 52XH had 12.1% EL, and therefore low EL cannot be satisfactorily explained by PAGS alone.

The difference between 47VH and 52XH is the vanadium addition. Using the Orowan equation, it could be shown that a smaller precipitate strengthens more. During cooling, VC formed random precipitation or interphase precipitation in ferrite or pearlite, and the precipitates were very small, typically of <10nm in size. Those precipitates should greatly contribute to strengthening, as shown in Figure 1. However, hot forged work pieces practically contain macrosegregation and are inherently inhomogeneous in the microstructure. It was very difficult to quantify the size and distribution of nano-sized VC in 47VL and 47VH. Therefore, we took a different approach and studied the undissolved MCN.

For 47V, Thermal-Calc calculations showed that MCN almost dissolves at around 1100ºC, and the elements in the MCN differ significantly with temperature, illustrated in Figure 4. VC is the primary constituent of MCN at about 900ºC, whereas MCN is mainly composed of TiN at 1100ºC. As the reheat temperature range was between 1000-1200ºC, it was expected that there would be differences in the characteristics of MCN. TEM experiments were conducted to identify the differences in MCN of 47VH and 47VL. Figure 5 shows 47VL has higher amounts of large undissolved MCN, while 47VH has fewer. As the reheat temperature increased, more MCN dissolved. To further identify the differences in MCN, the chemistry of the MCN precipitates was evaluated. Typical EDS results showed Ti, V, N, C, Fe signals, and Fe and C were filtered out as the Fe signal could come from a matrix, while the C signal was from a carbon replica. As MCN is an FCC lattice, total M sites are equal to V_{af}+Ti_{af} sites, and also equal to C+N sites. Therefore, V has a site fraction of $V_{af}/(V_{af}+Ti_{af})$, and N has a site fraction of $N_{af}/(V_{af}+Ti_{af})$, where V_{af}, Ti_{af}, and N_{af} are atomic fractions measured from the EDS signal, respectively. Ti, V, and N signals were evaluated using calculated site fractions, and the EDS data are shown in Figure 6. As shown, there is a clear distinction in the precipitates. Compared to 47VL, it can be seen that the MCN precipitates in 47VH have lower V (i.e., higher Ti)

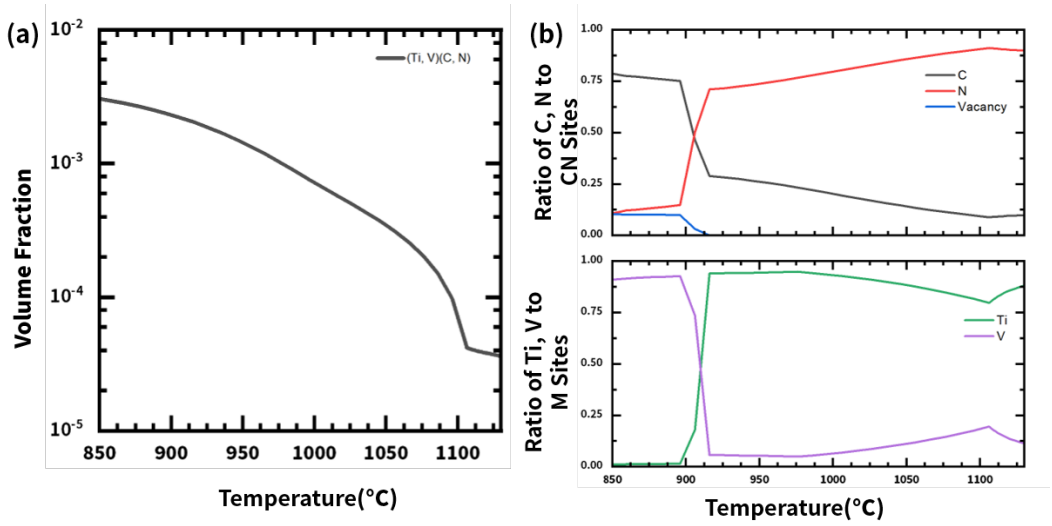

Fig.4. (a) The volume fraction of MCN precipitation as a function of temperature, and (b) the composition of precipitates, calculated using ThermalCalc.

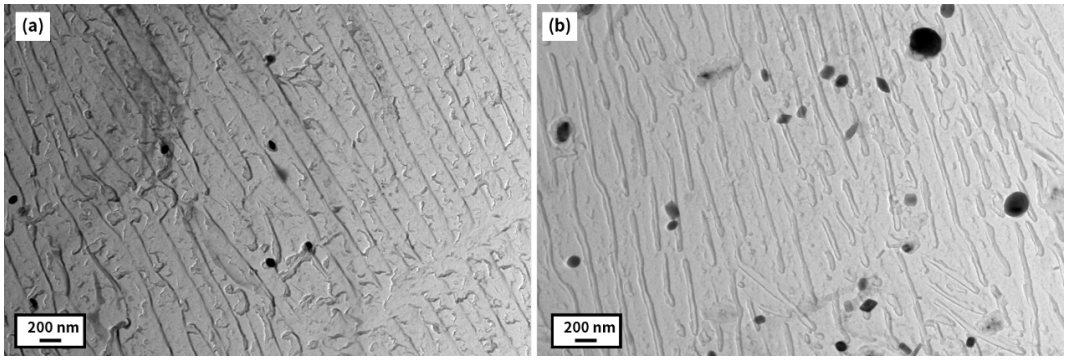

Fig.5. TEM micrographs showing the distribution of undissolved MCN in **(a)** 47VH and **(b)** 47VL.

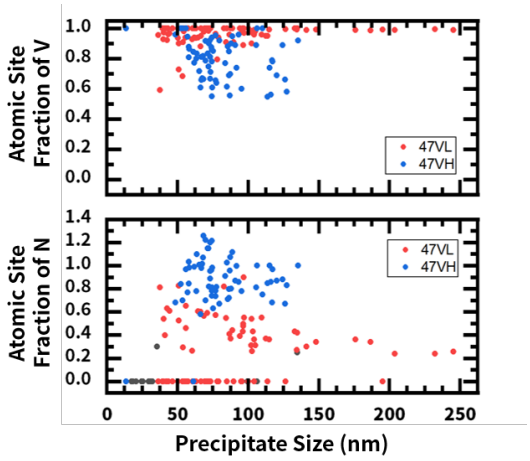

Fig.6. The atomic site fraction of V and N measured using EDS.

and higher N. As shown in Figure 4(a)(b), ThermalCalc indicates that at higher temperatures, precipitate dissolution occurs, and the remaining undissolved precipitates are enriched in Ti and N. On the other hand, for 47VL, precipitate compositions correspond to that of a lower temperature. Notably, the precipitates of 47VL and 47VH are both enriched in V, and V compositions (at least 60%) are significantly higher than that calculated by ThermalCalc (10-20% when temperature is between 1000-1200ºC). It is reasonable to assume that during cooling, VC precipitation occurred, and some VC attached to existing MCN precipitates as there was no nucleation barrier, increasing the V fraction in the MCN. Future experiments using interrupted quenching can be conducted to verify the hypothesis. Based on these results, it is reasonable to assume that, 47VL has more undissolved MCN precipitates, and MCN acted as a vanadium sink during cooling, evidenced by higher V in MCN. Therefore, 47VL had less vanadium available to form small VC precipitates.

Previous research indicated that after deformation, the pearlitic structure showed a characteristic stripe structure, as shown in Figure 7. Miller and Smith explained the stripe formation mechanism as follows[6]. Under shear, deformation concentrates on shear bands. As shear bands pass through pearlitic ferrite and pearlitic cementite, accumulated strain shears the lamellar structure, and voids form at the intersection of the shear band and cementite lamellae. As strain increases, the void can extend and connect with adjacent voids, creating a series of microcracks, that appear as stripes.

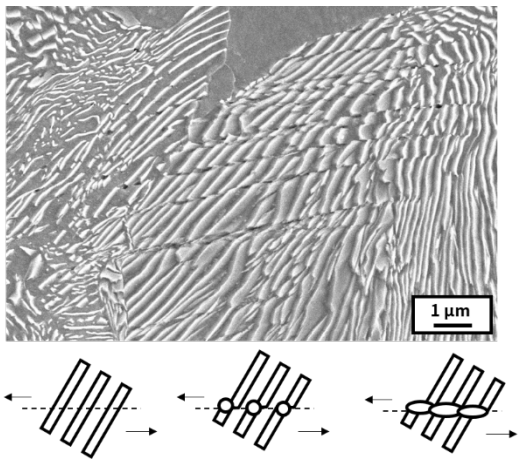

Fig.7. SEM micrograph of shear band in pearlite and Miller-Smith mechanism.

As illustrated in Figure 8, the mechanism of tensile fracture in vanadium-alloyed steel can be inferred as follows. Fracture is compulsory debonding of atoms, and therefore, the site with the weakest atomic bonding is the

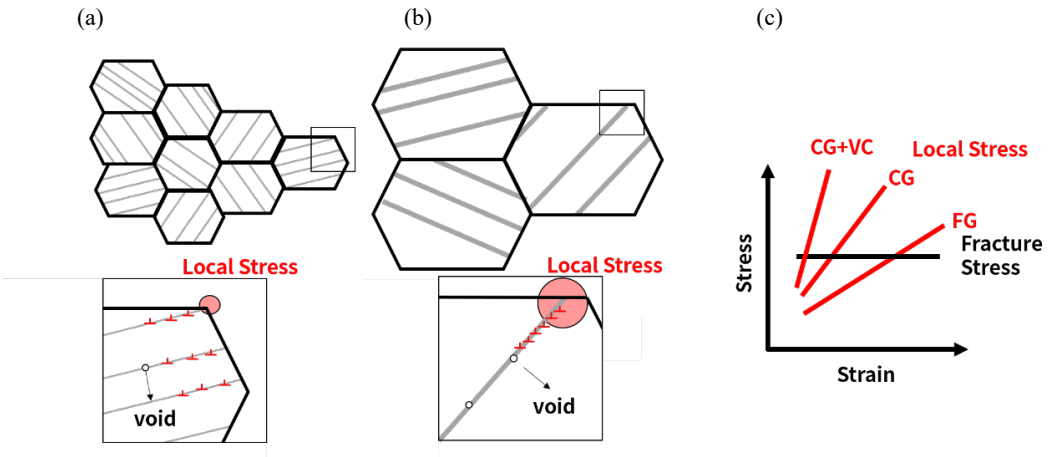

Fig.8. The mechanism of elongation loss. (a) Fine PAG (FG). (b) Coarse PAG (CG). The gray line indicates the shear band undergoing the Miller-Smith mechanism. (c) Stress-strain plot of local stress and fracture stress. VC denotes steels with VC precipitation.

crack nucleation site and is usually matrix/inclusion interfaces or PAG boundaries. Here we only consider PAG boundaries. The bonding strength is related only to the elements of and the distance between adjacent atoms (i.e. atomic scale) and is therefore indifferent to macroscopic strain. In Figure 8(c), bonding strength is depicted as a horizontal line in the stress-strain plot and is also called fracture stress. As plastic strain increases, work hardening leads to increased local stress. When maximum local stress is still below fracture stress, plastic deformation continues, leading to further work hardening. If maximum local stress is larger than fracture stress, atomic debonding occurs, nucleating cracks. Cracks can be arrested if plastic deformation blunt the crack tip, however, for pearlitic steels, because of the Miller-Smith mechanism, in pearlite there are already stripes of microcracks, assisting crack propagation. As a result, we can assume that, for pearlitic steel, when local maximum stress exceeds fracture stress, cracks occur and easily propagate, and UTS is achieved.

Figure 8(a) shows that, when PAG is fine, shear bands homogeneously distribute in multiple grains. Microscopically, shear bands are high-density dislocations, that cannot pass austenite grain boundaries, and therefore, dislocations accumulate at the intersections, leading to higher local stress. As strain increases, we assume local stress also increases linearly, and the local stress plot, denoted as FG, is illustrated as a straight line in Figure 8(c). On the other hand, we can expect a larger shear band for a coarse PAG. Compared to its fine-grained counterpart, more dislocations accumulate, leading to a steeper slope of the local stress plot (CG) in Figure 8(c). As explained, the intersection of local stress and fracture stress marks EL, and therefore coarse PAG has smaller EL. If there are VC precipitates, because of the Orowan effect, dislocations interact with precipitates, forming a dislocation loop and causing dislocation-multiplication, resulting in a greater work hardening effect. Combined with coarse PAG, the stress-strain plot has an even steeper slope (CG+VC), resulting in abnormally low EL found in vanadium-alloyed medium-carbon steel.

In summary, high reheat temperature results in coarsened PAG as well as enhanced VC precipitation during cooling, and is presumably the cause of the loss in elongation. It is suggested that the reheating temperature be carefully controlled to prevent this issue.

4. CONCLUSIONS

Tensile results showed that 47VL and 47VH had elongations of 11.9% and 2-3%, respectively. Fractography showed that the unit of cleavage fracture is prior austenite grain (PAG) and prior austenite deviate crack propagation. Microscopy results showed that the main differences between the two samples were the size of the PAG and the distribution of undissolved precipitation. With a higher reheat temperature of 47VH, a higher amount of vanadium was in solution, and VC precipitated more when the forged workpiece cooled to room temperature.

Miller-Smith's mechanism indicates that the deformation structure of pearlite consists of strip-like voids, assisting crack propagation. It is concluded that, given the same strain amount, 47VH had higher local stress because of large PAG and VC precipitates, which accelerated dislocation multiplication, and therefore cracks were easier to nucleate at the intersection of the shear band and PAG boundary. Because cracks easily initiate and propagate, 47VH has reduced elongation. A lowered reheating temperature could prevent the issue by refining PAG and reducing VC precipitation during cooling.

REFERENCES

1. D. K. Matlock and J.G. Speer: Mater. Sci. Technol. 2009, vol.25, pp. 1118-1125.
2. R. A. Grange, C. R. Hribal, L. F. Porter: Metall. Mater. Trans. A 1977, vol.8, pp.1775-1785.
3. T. N. Baker: Ironmaking Steelmaking 2016, vol.43, pp. 264-307.
4. G. Miyamoto, R. Hori, B. Poorganji, T. Furuhara: ISIJ Int. 2011, vol.51, pp. 1733-1739.
5. G. L. Dunlop, C.J. Carlsson, G. Frimodig: Metall. Mater. Trans. A 1978, vol.9, pp. 261-266.
6. J. Toribio, B. González, J.C. Matos, F.J. Ayaso: Metals 2016, vol.6, p.318.